Efficiency comparison between integrated optical waveguide probes and conventional fiber probes in the detection of backscattered light

N. Ismail, F. Sun, F. Civitci, K. Wörhoff, R. M. de Ridder, M. Pollnau, and A. Driessen

Integrated Optical Micro Systems Group, MESA+ Institute for Nanotechnology,
University of Twente, P.O. Box 217, 7500 AE Enschede, The Netherlands
n.ismail@ewi.utwente.nl

Abstract. *Multimode silicon-oxynitride (SiON) waveguide structures are investigated for probing fluorescence and backscattered light from samples of different thicknesses. The collection efficiency together with the resolution of such probes is compared to that of a conventional fiber probe. The simulation results show that, in case of low scattering samples, among the two types of probes the former present higher collection efficiencies when the sample thickness is below 85 µm. The analytical model developed to estimate the collection efficiency of the integrated probes was validated experimentally through fluorescence measurements carried out on a ruby rod. The model and the experimental results are both presented in this work.*

Introduction

Fiber probes are widely used today as non-invasive tools for medical diagnosis. Different probe geometries have been extensively studied and characterized by many researchers. In particular, a first theoretical model was introduced by Schwab et al. [1] and Plaza et al. [2], then extended by Cooney et al. [3] to compare different Raman probe designs.

In this work we investigate the use of integrated optical waveguide probes and compare their collection efficiency with that of conventional fiber probes for the detection of light from thin samples. Among the advantages of integrated probes are the possibility to investigate very small volumes, the polarization maintenance, and the extremely reduced propagation length compared to that of a fiber. Another considerable advantage is that, depending on the technology, integrated probes can be placed on the same chip together with filters and other wavelength selective devices, and by hybrid integration even with detectors and the necessary electronic circuits.

Analytical model of waveguide probes

In order to model integrated waveguide probes we consider as a starting point the model of a dual-fiber probe introduced by Cooney et al. [3]. The schematic of the probe is shown in Fig 1. The probe is positioned at a distance D from the surface of the sample under study and is composed of one excitation fiber and one collection fiber, spaced a distance d apart. We only treat the simple case in which the material between probe and sample has the same refractive index as the sample. P_e is the power coupled into the excitation fiber, while P_c is the power collected by the collector fiber. In our case, instead of the fibers, we will consider integrated waveguides with rectangular cross-section. The light exiting the excitation waveguide will form an elliptical cone of light entering the sample, since the diffraction in the horizontal and vertical directions are in general different. Similarly, the collector waveguide will have an elliptical acceptance

cone. The overlap region between the two cones determines the collection efficiency or "figure of merit" of the probe, and its volume V is highly dependent on the numerical apertures of excitation and collection waveguides, and also on the distance D between probe and sample.

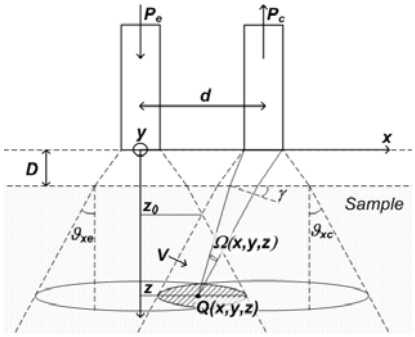

Fig 1. Schematic of excitation and collection waveguides separated by the distance d. P_e is the power coupled into the source waveguide and P_c is the power coupled back into the collector waveguide.

To estimate the figure of merit S, we compute the total power collected by the probe by integrating the power collected from each point Q inside the overlap volume V. In case of integrated probes we have to face the fact that many approximations that were valid for fiber probes cannot be applied any longer. The main differences are that integrated waveguides in general present only a few number of modes compared to the quasi-continuum of modes of a large-core fiber, and that the shape of the waveguides is rectangular giving rise to an elliptical shape of the effective cross-section or collection area. Once the effective cross-section has been determined, we then compute the solid angle Ω subtended by this elliptical area at each point Q of the overlap volume V by discretizing the ellipse and applying the exact formula proposed by Asvestas and Englund for computing the solid angle subtended by a planar figure [4].

To correctly determine the shape of both the exit and acceptance cones, and therefore the overlap volume V, we must estimate the correct values of the exit angles of the excitation waveguide in both the horizontal and vertical directions, and the acceptance angles of the collector waveguide. It is important to note that -for multimode channels- the exit angles of the excitation waveguide are in general different from the acceptance angles of the collector waveguide even in the case that both waveguides present the same cross-section. This can be understood by keeping in mind that when coupling light into the source waveguide we can excite different combinations of modes depending on both the alignment between the input fiber and the waveguide, and the mode profile of the input fiber. For this reason we directly measure the exit angles from the excitation waveguide by placing an opaque screen in front of the waveguide output facet and a camera focused on the screen. The camera is used to measure the spot size for two different distances of the screen from the waveguide facet. Each spot is approximated with a Gaussian profile, and the spot size is estimated in both horizontal and vertical directions by considering the points where the intensity decays below $1/e^2$ of the maximum. For estimating the acceptance cone of the collector waveguide we apply a numerical procedure: we calculate the overlap integral between a plane wave, incident at an angle ϑ on the waveguide facet, and each of the guided modes in order to obtain the total power coupled into the waveguide for a given angle of incidence.

The figure of merit S [sr·m], which allows comparing different probe configurations, is defined by the power collected by the probe from the overlap volume V divided by the quantity $P_e\beta N$; where β is the differential scattering cross-section [m^2sr^{-1}], and N is the number of scattering molecules per unit volume [m^{-3}]. In this way we obtain a quantity that is independent of the scattering properties of the sample and the input power, but only depends on the geometry of the probe and the overlap volume:

$$S = \iiint_V \frac{T_e T_c \Omega(x,y,z)}{\pi \sigma_x(z)\sigma_y(z)} \exp\left(\frac{-x^2}{\sigma_x^2(z)} + \frac{-y^2}{\sigma_y^2(z)} \right) dxdydz \,. \quad (1)$$

In (1) T_e is the fraction of the input power P_e that enters the sample, while T_c is the fraction of the power that reaches the collector waveguide facet from point Q, and that is coupled into the collector waveguide. The variances σ_x and σ_y define the Gaussian intensity profile of the excitation light at depth z inside the sample; they are strictly related to the exit angles of the source waveguide along the horizontal and vertical directions, respectively.

Efficiency comparison between integrated probes and fiber probes

The integral in (1) was evaluated numerically for an integrated probe positioned in contact with the sample, for different sample thicknesses. We considered SiON waveguides with a cross-section of 5 μm × 0.82 μm, and SiO_2 cladding and separation of d = 11 μm. We compared these probes with typical Raman dual-fiber probe with core radii of 100 μm, and separation d = 210 μm. The simulation results for the two kinds of probes are shown in Fig 2. The figure of merit for the fiber probes was calculated both using our model and the mathematical model presented in the work of Cooney et al. [3] which makes use of an approximated expression for the solid angle Ω.

It becomes clear from Fig. 2 (a) that integrated waveguide probes provide efficiencies exceeding those of conventional fiber probes in case of thin samples (thicknesses t < 85 μm).

Another advantage of integrated probes over fiber probes is the smaller collection volumes and, thus, higher resolution, as can be seen from the results shown in Fig 2 (b).

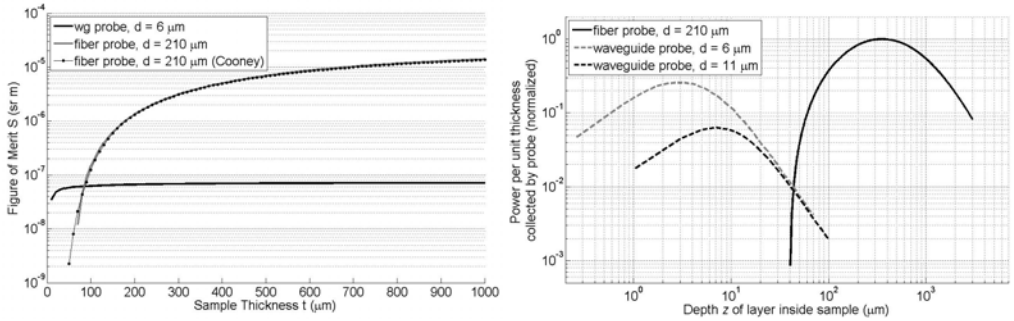

(a) **(b)**

Fig 2. (a) Figure of merit S as a function of the sample thickness t for an integrated dual-waveguide probe with cross-sections 5 μm × 820 nm and distance d = 6 μm (solid line), compared to that of a dual-fiber probe with core radii of 100 μm and distance d = 210 μm (dashed line). (b) Power per unit thickness collected by a probe from a layer situated inside the sample as a function of layer depth.

Experimental results

To validate the analytical model we performed fluorescence measurements on a ruby rod using the experimental arrangement shown in Fig 3 (a), in which an integrated probe with multiple collection waveguides was used in order to measure the fluorescent signal as a function of distance from the excitation point.

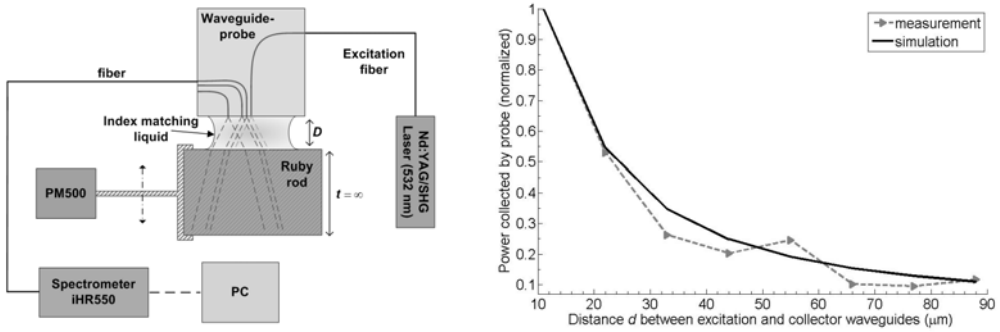

Fig 3. (a) Setup for the measurement of fluorescence from a ruby rod. (b) Fluorescence measured by a waveguide probe as a function of the distance *d* between excitation and collector waveguides. Comparison of experimental and simulation results

The good agreement between simulation and experimental results, shown in Fig 3 (b), validates our analytical model.

Conclusions

We developed an analytical model for describing waveguide probes, which is valid for single-mode as well as multi-mode waveguides with arbitrary cross-sections. With the help of our model we have demonstrated that integrated probes present higher efficiencies compared to conventional fiber probes in case of thin samples and that they reach higher resolutions having a smaller collection volume than that of a fiber probe. The model has been validated by our experimental results.

Acknowledgment

We gratefully acknowledge financial support from the IOP Photonic Devices supported by the Dutch funding agencies Senter-Novem and STW and the European Network of Excellence ePIXnet.

References

[1] S. D. Schwab and R. L. McCreery, "Versatile, efficient Raman sampling with fiber optics," *Analytical Chemistry*, vol. 56, pp. 2199-2204, 1984.

[2] P. Plaza, N. Q. Dao, M. Jouan, H. Fevrier, and H. Saisse, "Simulation et optimisation des capteurs a fibres optiques adjacentes," *Applied Optics*, vol. 25, pp. 3448-3454, 1986.

[3] T. F. Cooney, H. T. Skinner, and S. M. Angel, "Comparative study of some fiber-optic remote Raman probe designs. Part I: Model for liquids and transparent solids," *Applied Spectroscopy*, vol. 50, pp. 836-848, 1996.

[4] J. S. Asvestas and D. C. Englund, "Computing the solid angle subtended by a planar figure," *Optical Engineering*, vol. 33, pp. 4055-4059, 1994.